Title

Layered SnS2-Reduced Graphene Oxide Composite – A High-Capacity, High-Rate, and Long-Cycle Life Sodium-Ion Battery Anode Material

Journal

Advanced Materials, 26(23)

ISSN

0935-9648

Authors

Qu, Baihua
Ma, Chuze
Ji, Ge
et al.

Publication Date

2014-06-01

DOI

10.1002/adma.201306314

Peer reviewed

Layered SnS_2-Reduced Graphene Oxide Composite – A High-Capacity, High-Rate, and Long-Cycle Life Sodium-Ion Battery Anode Material

Baihua Qu, Chuze Ma, Ge Ji, Chaohe Xu, Jing Xu, Ying Shirley Meng, Taihong Wang, and Jim Yang Lee**

The idea of sodium-ion batteries (NIBs) as a substitute of lithium-ion batteries (LIBs) for grid-scale energy storage was initially driven by cost considerations.[1] Research in the last several years has shown that NIBs are not necessarily deficient in performance.[2] Hence there is a strong current interest in developing high-performance NIB anode[3] and cathode[4] materials. Thus far tin and tin-based compounds have shown good prospect as high-capacity NIB anodes based on the theoretical stoichiometry of $Na_{15}Sn_4$ (847 mAh g^{-1}).[5–15] For example, Liu et al.[9] reported initial capacity of 722 mAh g^{-1} and capacity of 405 mAh g^{-1} after 150 cycles at 50 mA g^{-1} for a composite Sn anode consisting of an array of nanorods with a carbon outer shell, a Sn intermediate layer and a metal inner core (3D Sn nanoforests). Anodes which were based on SnO_2 (432 mAh g^{-1} after 150 cycles at 20 mA g^{-1})[10] and SnO_2@graphene nanocomposite (638 mAh g^{-1} after 100 cycles at 20 mA g^{-1})[11] have also been demonstrated. Wu and co-workers[12] examined Sn–SnS–C nanocomposites as NIB anodes and reported reversible capacities of 664 mAh g^{-1} at 20 mA g^{-1} and 350 mAh g^{-1} at 800 mA g^{-1}. These are clearly encouraging developments but a high-capacity tin-based anode with good rate performance and long cycle life has yet to be identified. The lack of cycle stability is often attributed to the deleterious volume expansion in tin-sodium alloy formation (a 420% volume expansion upon the formation of $Na_{15}Sn_4$) resulting in electrode disintegration and gradual loss of electrical contact with the current collector.[13,16] The situation is similar to the early days of the development of alloy anodes for the LIBs. Considerable improvements in the design and optimization of anode composition and structure are still required.

This note reports our design and implementation of a SnS_2-based nanocomposite anode for the NIBs. SnS_2 has a CdI_2-type of layered structure (a = 0.3648 nm, c = 0.5899 nm, space group P3m1) consisting of a layer of tin atoms sandwiched between two layers of hexagonally close packed sulfur atoms. This layered structure with a large interlayer spacing (c = 0.5899 nm) should easy the insertion and extraction of guest species and adapt more easily to the volume changes in the host during cycling. This has been confirmed by the performance of SnS_2 as a reversible lithium storage host in several studies.[17] The electrochemical properties of layered sulfides (SnS_2, MoS_2, WS_2) were further improved by integration with graphene. The structural compatibility between the two layered compounds and the good electronic properties of graphene led to very stable composites (i.e. long cycle-life) with high reversible capacity and good rate performance in LIB applications.[18] The SnS_2 layer structure should also be viable for reversible Na^+ storage since, in comparison with tin and other tin-based materials, it has the largest buffer for the volume changes in Na-Sn reactions. The LIB developmental efforts also suggest layer-structured SnS_2-reduced graphene oxide (SnS_2-RGO) nanocomposites as an improved version of the SnS_2 anode.

The design of the SnS_2-RGO hybrid structure for reversible storage of Na^+ was based on the following materials principles: 1) a large interlayer spacing in the SnS_2 structure benefiting Na^+ intercalation and diffusion, and more buffering space for beneficial adjustment the volume changes in the host during cycling; 2) fast collection and conduction of electrons through a highly conductive RGO network; and 3) inhibition of Sn (Na_xSn) aggregation during cycling by RGO after material hybridization. The experimental results validated the expectations: the SnS_2-RGO anode delivered a high charge (desodiation) specific capacity of 630 mAh g^{-1} at 0.2 A g^{-1}, and more impressively, 544 mAh g^{-1} after a ten-fold increase in current density to 2 A g^{-1}. The electrode was also very stable to cycling; providing a nearly unvarying capacity of 500 mAh g^{-1} at 1 A g^{-1} even after 400 charge-discharge cycles.

The SnS_2-RGO nanocomposite was produced by a facile hydrothermal route from a mixture of tin (IV) chloride, thioacetamide (TAA) and graphene oxide (GO) (details in the Experimental Section). In the comparison of the X-ray diffraction (XRD) patterns of the SnS_2-RGO composite, SnS_2 and GO in **Figure 1**a, GO only displayed a single diffraction peak at 10.9° from the (002) planes.[19] The powder XRD patterns of SnS_2 and

B. Qu, Prof. T. Wang
Key Laboratory for Micro-Nano Optoelectronic Devices of Ministry of Education and State Key Laboratory of Chemo/Biosensing and Chemometrics
Hunan University
Changsha 410082, P. R. China
E-mail: thwang@hnu.edu.cn
B. Qu, Dr. G. Ji, Dr. C. Xu, Prof. J. Y. Lee
Department of Chemical and Biomolecular Engineering
National University of Singapore
10 Kent Ridge Crescent 119260, Singapore
E-mail: cheleejy@nus.edu.sg
C. Ma, J. Xu, Dr. Y. S. Meng
Department of NanoEngineering
University of California
San Diego, La Jolla, CA 92037, USA

DOI: 10.1002/adma.201306314

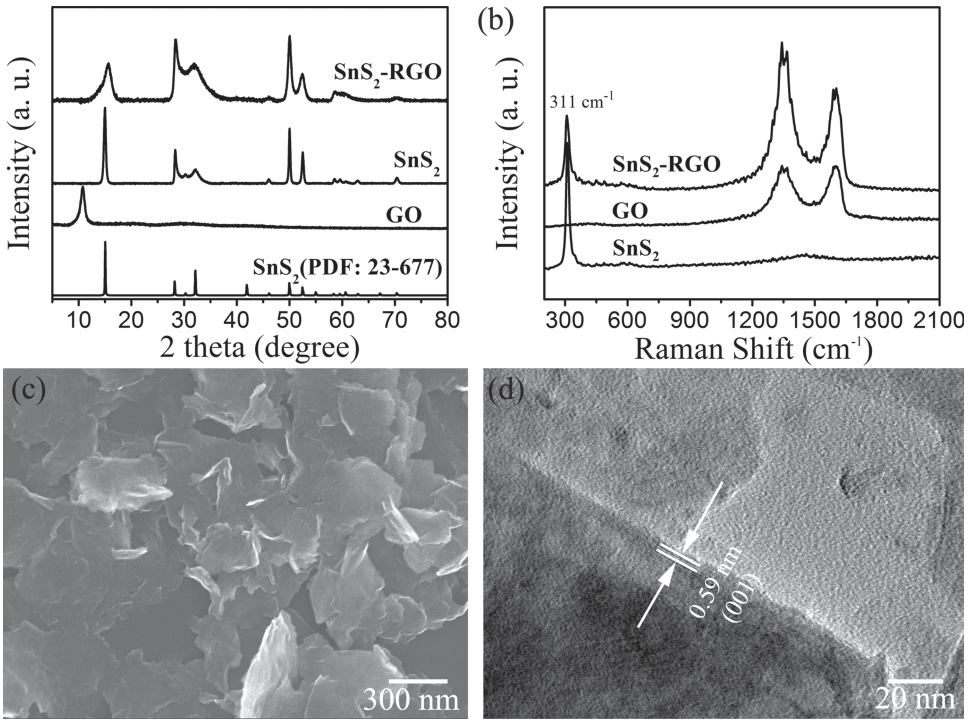

Figure 1. a) XRD patterns. (b) Raman spectra of SnS_2, GO, and the SnS_2-RGO composite. c) A representative FESEM image of the SnS_2-RGO composite. d) A HRTEM image of the SnS_2-RGO composite.

SnS_2-RGO index well with the 2T-type layered structure (space group: P3m1, JCPDS card no. 23–677);[17] and there was no significant impurity in the composite. The absence of the GO peak at 10.9° in the XRD pattern of SnS_2-RGO confirms the formation of RGO during the hydrothermal treatment.[18b] The GO, SnS_2 and SnS_2-RGO samples were also characterized by Raman spectroscopy (Figure 1b). GO could be characterized by the graphitic-G band at ~ 1350 cm^{-1} and the disorder-induced D band at ~ 1580 cm^{-1}. SnS_2 could be characterized by a peak at 311 cm^{-1} corresponding to the A_{1g} mode of SnS_2,[18a,b,20] which was present in the spectra of SnS_2 and SnS_2-RGO. The intensity ratio of the D-band to G-band of GO (I_D/I_G) was higher in SnS_2-RGO; indicating a reduction in the average size of the sp_2 domains after GO reduction.[21] The field-emission scanning electron microscopy (FESEM) image of the SnS_2-RGO composite (Figure 1c) shows a homogeneous structure with many large but thin sheets (several hundred nanometers in size). High resolution transmission electron microscopy (HRTEM) revealed the composite nature of the sheets consisting of a distributed of the SnS_2 nanosheets (~10 layers) among the RGO sheets. Figure 1d shows the interplanar spacing of 0.59 nm corresponding well with the (001) plane of 2T-type layered structure SnS_2.

Cyclic voltammetry (CV) was performed in the 0 to 2.5 V potential region at 0.1 mV s^{-1} (**Figure 2**a). Although the storage mechanism has yet to be exactly known, there are some consensuses about the common voltammetric features: The very broad peak at 1.5~1.7 V in the first cathodic process (reduction) is commonly assigned to sodium intercalation of the SnS_2 layers without phase decomposition (similar to the lithium intercalation of the SnS_2 layers).[17d] The sharp and intense cathodic peak at ~0.55 V could be attributed to conversion and alloying reactions. As well as the formation of irreversible solid electrolyte interphase (SEI) in the 1st cycle. Indeed the cathodic peak at ~0.55 V was replaced by two peaks at ~0.62 and ~0.9 V in subsequent cycles, an indication of the good reversibility and predominance of the storage reactions after a stable SEI had been formed in the 1st cycle. In the anodic scan, the inconspicuous oxidation peaks at ~0.3 and ~0.75 V in all cycles may be attributed to the desodiation reaction of Na_xSn. The distinct oxidation peak at ~1.2 V may correspond to the restitution of the original SnS_2-RGO. The voltammograms were superimposable after the first cycle; indicating very good reversibility of SnS_2-RGO for the sodiation and desodiation reactions.

On deep galvanostatic cycling between 0.01 and 2.5 V, the discharge (sodiation) capacity was 839 mAh g^{-1} and the charge (desodiation) capacity was 630 mAh g^{-1} in the first cycle at a current density of 0.2 A g^{-1}.The first cycle irreversible capacity loss of 209 mAh g^{-1} (25%) could be attributed mainly to SEI formation (Figure 2b). The electrode showed good cycle stability from the 2nd cycle onwards, delivering discharge capacities of 645, 654, 628 mAh g^{-1} in the 2nd, 20th and 100th cycle respectively. The overlapping voltage profiles in Figure 2b demonstrate the excellent electrochemical reversibility during cycling sustaining a coulombic efficiency of >99% from the 2nd cycle onwards (Figure S3). For comparison the performance of SnS_2 and RGO was also measured under identical test conditions as shown in Figure 2c. It was confirmed that RGO contributed negligibly to Na^+ storage (~30 mAh g^{-1}). For the SnS_2 electrode, not only was its specific capacity significantly lower than the SnS_2-RGO electrode, there was also severe capacity fading resulting in a

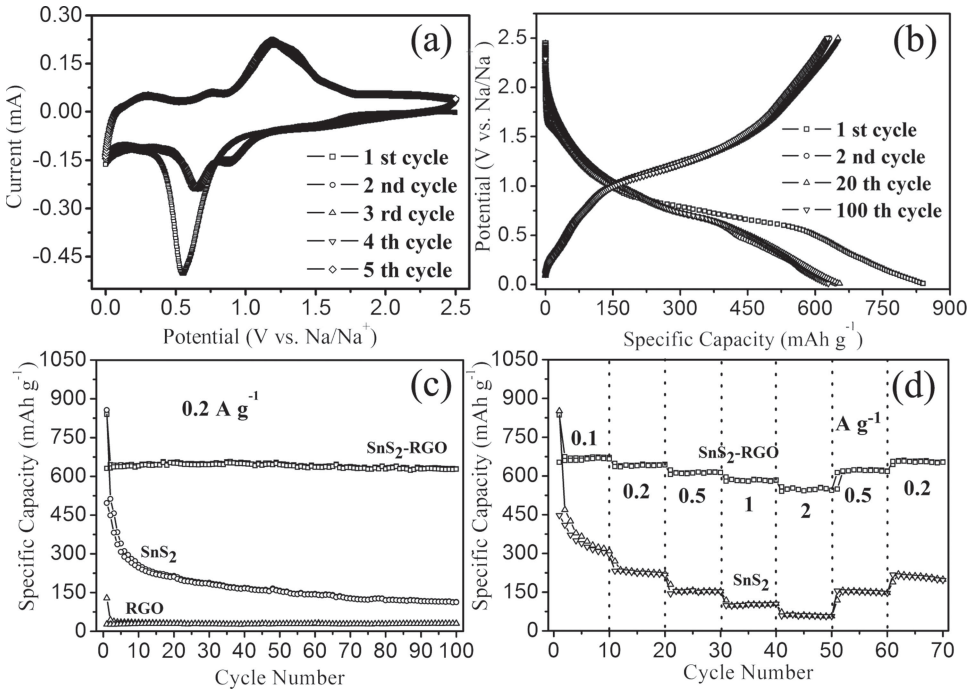

Figure 2. a) The first five cycle voltammograms of the SnS_2-RGO electrode at 0.1 mV s^{-1}. b) Voltage profiles of a SnS_2-RGO electrode in the 1st, 2nd, 20th and 100th cycles. c) Cycling performance of SnS_2-RGO, SnS_2 and graphene electrodes at 0.2 A g^{-1} for 100 cycles, respectively. d) Rate performance of SnS_2-RGO and SnS_2 electrodes.

discharge capacity of only 113 mAh g^{-1} after 100 cycles. Severe capacity fading could be due to the low electronic conductivity of unsupported SnS_2 and un-restrained aggregations of Sn (or Na_xSn) during cycling. The voltage profiles of the SnS_2 and RGO electrodes in the selected number of cycles can be found in Figure S1 and Figure S2.

The rate capability of the anode material is an important performance indicator for grid-scale electricity storage and electric vehicle applications. Figure 2d shows the rate capability of SnS_2 and SnS_2-RGO from 0.1 to 2 A g^{-1}. The SnS_2-RGO electrode was clearly superior by comparison. The test began with the current density of 0.1 A g^{-1}, where the discharge capacity of the SnS_2-RGO electrode was consistently ~ 670 mAh g^{-1} for the first ten cycle. When the current density was increased in steps to 0.2, 0.5, and 1.0 A g^{-1}, the capacity decrease was very small for a battery material. Even after a 20 fold increase in current density to 2.0 A g^{-1}, a discharge capacity of ~544 mAh g^{-1} or 81% of the capacity at 0.1 A g^{-1} (671 mAh g^{-1}), could still be retained. The discharge capacities when the current density was returned to 0.5 and 0.2 A g^{-1} were ~620 and ~650 mAh g^{-1}, which were only marginally lower than the values before the current density increase. The negligible changes in discharge capacity with current density changes indicate the resilience of the SnS_2-RGO hybrid structure. Evidently the large interlayer spacing allowed Na^+ transport to be carried out at high rates (high current densities) without causing irreversible changes to the hybrid structure. The typical voltage profiles of the SnS_2-RGO electrode at 0.1, 0.2, 0.5, 1.0, and 2.0 A g^{-1} rates could be found in Figure S4.

For the evaluation of the long-term cycle stability of the SnS_2-RGO electrode, the electrode was galvanostatically discharged and charged at 0.2 A g^{-1} for the first five cycles; and then at 1 A g^{-1} for 400 cycles (**Figure 3**a). The discharge capacity of 594 mAh g^{-1} in the 6th cycle at 1 A g^{-1} was used as the baseline. The capacities at the end of 50, 100, 200 and 400 cycles were 566 mAh g^{-1} (95%), 565 mAh g^{-1} (95%), 552 mAh g^{-1} (93%) and 500 mAh g^{-1} (84%) respectively. The performance surpasses any other NIB anode reported in the literature to date (Table S1). There was practically no capacity decrease in the first two hundred cycles. The superior cycle stability of the SnS_2-RGO electrode for reversible Na^+ storage was highly repeatable. We have tested three different batches of SnS_2-RGO electrodes and the results are shown in Figure 3b and 3c. Figure 3b shows the overlapping voltage profiles of these electrodes in the 200th cycle. The cycling performance of the three different SnS_2-RGO electrodes was also perfectly superimposable under the same test conditions (Figure 3c).

To further confirmations of the practically of the SnS_2-RGO composite for NIBs applications, the SnS_2-RGO anode was paired up with P_2 phase $Na_{0.80}Li_{0.12}Ni_{0.22}Mn_{0.66}O_2$ cathode, which has a theoretical capacity of 118 mAh g^{-1}, to form into a Na^+ full cell.[22] The active materials were loaded on the cathode and anode in the ratio of ~ 5.4:1 (mass loading of anode was 1.67 mg). The 1st, 2nd, 5th, 10th, and 15th cycle charge-discharge curves of the full cell are shown in **Figure 4**a. The first charge capacity was 1.106 mAh and the initial capacity loss was 0.398 mAh (36%). The full cell displayed relatively good stability, retaining 74% of the initial capacity after 50 cycles Figure 4b. The good coulombic efficiency was also replicated

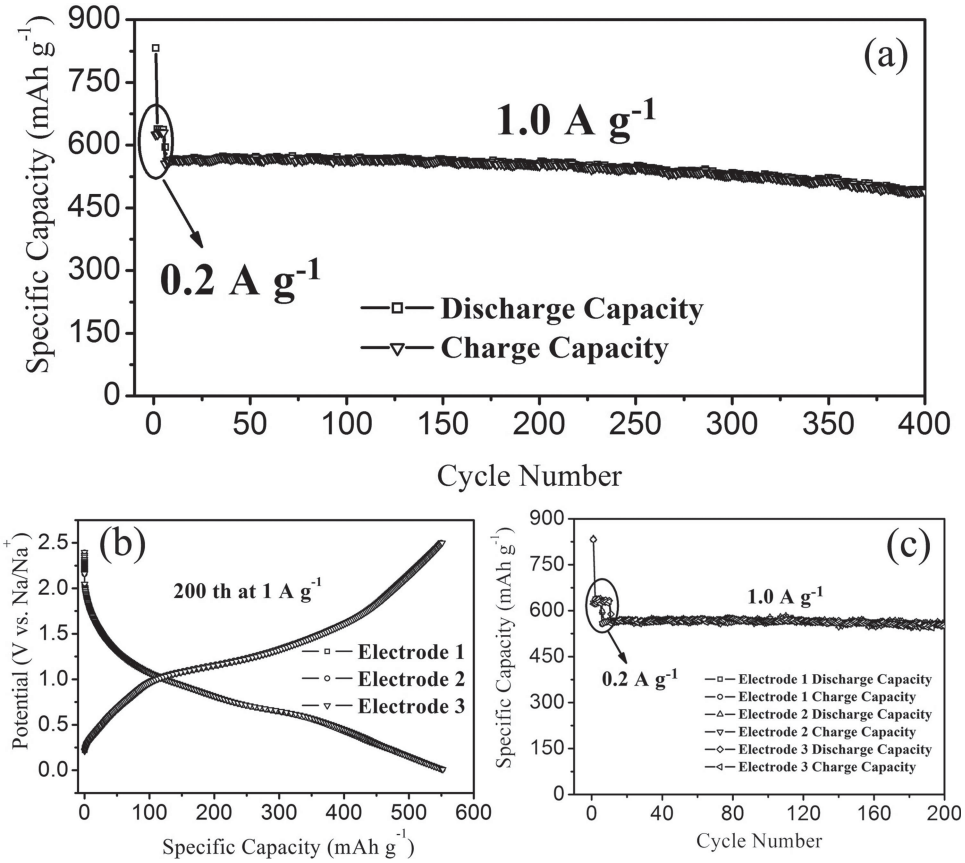

Figure 3. a) Long-term cycle stability of the SnS_2-RGO electrode (0.2 A g^{-1} for the first five cycles and 1 A g^{-1} for the next 400 cycles. b) Voltage profiles of the three different SnS_2-G electrodes in the 200th cycle. c) The cycle stability of three different batches of SnS_2-RGO electrodes.

in full cell studies (Figure S5). This preliminary data also represents the best of sodium-ion full cells reported to date.[3e,23] The greater capacity fading in the full cell was most likely caused by an un-optimized anode to cathode mass ratio; and the lack of match the of the C-rates between the two electrode materials. These parameters are difficult to optimize at the current stage of research.

In conclusion, we have developed a SnS_2-RGO composite with excellent electrochemical performance as the anode of NIBs. The SnS_2-RGO electrode demonstrated a high charge specific capacity (630 mAh g^{-1} at 0.2 A g^{-1}), good rate performance (544 mAh g^{-1} at 2 A g^{-1}) and long cycle-life (500 mAh g^{-1} at 1 A g^{-1} for 400 cycles). The excellent electrochemical performance could categorically be attributed to the SnS_2 layered structure where the increased interlayer spacing could better accommodate the volume change in Na-Sn insertion and de-insertions; and the good conductivity and mechanical resilience of RGO nanocomposites.

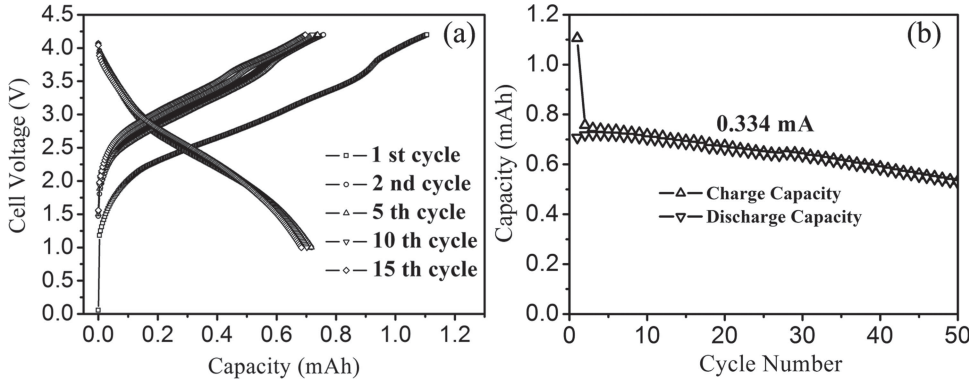

Figure 4. a) Voltage profiles of a full Na^+ cell consisting of $Na_{0.80}Li_{0.12}Ni_{0.22}Mn_{0.66}O_2$ cathode and SnS_2-RGO anode between 1.0 and 4.2 V at 0.334 mA. b) Cycling performance of the Na^+ full cell consisting of $Na_{0.80}Li_{0.12}Ni_{0.22}Mn_{0.66}O_2$ cathode and SnS_2-RGO anode.

Experimental Section

Materials Synthesis and Characterization: The graphite powder from Alfa Aesar, tin (IV) chloride pentahydrate ($SnCl_4$•$5H_2O$), thioacetamide (TAA) and carboxymethyl cellulose (CMC) from Sigma-Aldrich; and other analytical grade chemicals from various sources, were used as received without further purification. Deionized water was processed by Millipore Milli-Q to a resistivity of 18 MΩ cm^{-1} and higher. GO was prepared from the graphite powder by a modified Hummers' method,[24] as reported previously.[25] Exfoliation was carried out by sonicating a GO dispersion (1.5 mg ml^{-1}) under ambient conditions for 2 h. A typical synthesis of SnS_2-RGO composite is given as follows: 0.7015 g $SnCl_4$•$5H_2O$ (2 mmol) and 0.6014 g thioacetamide (TAA) (8 mmol) were added to 40 ml of 1.5 mg ml^{-1} GO suspension under stirring. The mixture was sonicated for 30 min before it was transferred to a 50ml Teflon-lined stainless steel autoclave, and heated at 160 °C for 12 h. After cooling to room temperature, the solid product was recovered by centrifugation, washed with deionized water and absolute alcohol thrice, and vacuum dried at 60 °C overnight. The dried product was then heated in Ar at the rate of 5 °C min^{-1} to 400 °C and kept at this temperature for 4 h. Pure SnS_2 was synthesized under the same conditions but without the presence of GO. RGO was obtained by treating GO in an Ar/H_2 (5%) mixture at 800 °C for 20 min. All solid products prepared above were characterized by field-emission scanning electron microscopy (FESEM) on a JEOL JSM-6700F operating at 5 kV, by transmission electron microscopy (TEM) and High-resolution TEM (HRTEM) on a JEOL JEM-2010F operating at 200 kV, respectively. Powder X-ray diffractions (XRD) were recorded on a Shimadu XRD-6000 using Cu Kα radiation. Raman spectra were taken on a LabRAM HR 800 spectrometer at 633 nm.

Electrochemical Tests: For electrochemical measurements, 80wt% SnS_2-RGO (or SnS_2 or RGO), 10 wt% of conducting additive (acetylene black), and 10 wt% CMC were added to a distilled water-absolute alcohol mixture (3:2 by volume), and stirred for 8h to form a homogeneous slurry. The slurry was then applied to a copper foil and dried in vacuum at 80 °C overnight to form the working electrode. The test cells were coin cells (CR2032) which were assembled in an Ar-filled glove box (H_2O and O < 1ppm). Each cell typically contained 0.8–1 mg cm^{-1} of the active material. For half-cell studies the counter electrode was a sodium metal foil (Sigma-Aldrich) and a glass fiber GF/D (Whatman) filter was used as the separator. A 1 M solution of $NaClO_4$ (Sigma-Aldrich, 98%) in ethylene carbonate (EC)/diethylene carbonate (1:1 by volume) was prepared and used as the electrolyte. The cells were aged for 12 h before the measurements to ensure complete electrode wetting by the electrolyte. Galvanostatic discharge and charge at various current densities were performed on a battery tester (NEWARE BTS-5V, Neware Technology Co., Ltd.) with cut off potentials of 0.01 V for discharge and 2.5 V for charge. Cyclic voltammetry (CV) was performed on an AutoLab FRA2 type III electrochemical system at the scan rate of 0.1 mV s^{-1} at room temperature.

Full Cell Fabrication: A Swagelok cell was used as the full cell. The cathode was a mixture of $Na_{0.80}Li_{0.12}Ni_{0.22}Mn_{0.66}O_2$, acetylene black and poly(tetrafluoroethylene) (PTFE) in the weight ratio of 85:10:5. Anode preparation followed the same procedures as those used in the half-cell studies. The cathode to anode weight ratio was 5.4:1. The electrolyte was 1 M $NaPF_6$ in a 1:1 (v/v) mixture of ethylene carbonate (EC) and diethylene carbonate (DEC). The separator was a Whatman GF/D glass fiber filter paper. Battery assembly was carried out in an MBraun glovebox (H_2O and O < 1 ppm). Galvanostatic discharge and charge were performed on an Arbin BT2000 battery cycler between 1.0 – 4.2 V.

Supporting Information

Supporting Information is available from the Wiley Online Library or from the author.

Acknowledgements

This work was supported by a Scholarship Award for Excellent Doctoral Students from the Chinese Ministry of Education (2012). We thank the financial support of National Natural Science Foundation of China (Grant No. 61376073). C. Ma and Y. S. Meng acknowledge the funding support by USA National Science Foundation under Award Number 1057170. B. H. Qu would also like to acknowledge the China Scholarship Council (CSC) for providing his exchange scholarship for Ph. D. study at the National University of Singapore (NUS).

Received: December 30, 2013
Revised: February 25, 2014
Published online: March 27, 2014

[1] a) B. Dunn, H. Kamath, J. M. Tarascon, *Science* **2011**, *334*, 928; b) Z. G. Yang, J. L. Zhang, M. C. W. K. Meyer, X. C. Lu, D. W. Choi, J. P. Lemmon, J. Liu, *Chem. Rev.* **2011**, *111*, 3577.
[2] a) S. W. Kim, D. H. Seo, X. H. Ma, G. Ceder, K. Kang, *Adv. Energy Mater.* **2012**, *2*, 710; b) V. Palomares, P. Serras, I. Villaluenga, K. B. Hueso, J. C. Gonzalez, T. Rojo, *Energy Environ. Sci.* **2012**, *5*, 5884; c) M. D. Slater, D. Kim, E. Lee, C. S. Johnson, *Adv. Funct. Mater.* **2013**, *23*, 947; d) H. L. Pan, Y. S. Hu, L. Q. Chen, *Energy Environ. Sci.* **2013**, *6*, 2338.
[3] a) V. L. Chevrier, G. Ceder, *J. Electrochem. Soc.* **2011**, *158*, A1011; b) K. Tang, L. J. Fu, R. J. White, L. H. Yu, M. M. Titirici, M. Antonietti, J. Maier, *Adv. Energy Mater.* **2012**, *2*, 873; c) A. Darwiche, C. Marino, M. T. Sougrati, B. Fraisse, L. Stievano, L. Monconduit, *J. Am. Chem. Soc.* **2012**, *134*, 20805; d) Y. J. Kim, Y. W. Park, A. Choi, N. S. Choi, J. Kim, J. Lee, J. H. Ryu, S. M. Oh, K. T. Lee, *Adv. Mater.* **2013**, *25*, 3045; e) Y. S. Wang, X. Q. Yu, S. Y. Xu, J. M. Bai, R. J. Xiao, Y. S. Hu, H. Li, X. Q. Yang, L. Q. Chen, X. J. Huang, *Nat . Comm.* **2013**, *4*, 2365.
[4] a) Y. L. Cao, L. F. Xia, W. Wang, D. W. Choi, Z. M. Nie, J. G. Yu, L. V. Saraf, Z. G. Yang, J. Liu, *Adv. Mater.* **2011**, *23*, 3155; b) N. Yabuuchi, M. Kajiyama, J. Iwatate, H. Nishikawa, S. Hitomi, R. Okuyama, R. Usui, Y. Yamada, S. Komaba, *Nat. Mater.* **2012**, *11*, 512; c) Z. L. Jian, W. Z. Han, X. Lu, H. X. Yang, Y. S. Hu, J. Zhou, Z. B. Zhou, J. Q. Li, W. Chen, D. F. Chen, L. Q. Chen, *Adv. Energy Mater.* **2013**, *3*, 156; d) H. L. Chen, Q. Hao, O. Zivkovic, G. Hautier, L. S. Du, Y. Z. Tang, Y. Y. Hu, X. H. Ma, C. P. Grey, G. Ceder, *Chem. Mater.* **2013**, *25*, 2777; e) D. H. Lee, J. Xu, Y. S. Meng, *Phys. Chem. Chem. Phys.* **2013**, *15*, 3304; f) M. Guignard, C. Didier, J. Darriet, P. Bordet, E. Elkaïm, C. Delmas, *Nat . Mater.* **2013**, *12*, 74; g) L. Wang, Y. H. Lu, J. Liu, M. W. Xu, J. G. Cheng, D. W. Zhang, J. B. Goodenough, *Angew. Chem. Int. Ed.* **2013**, *52*, 1964.
[5] S. Komaba, Y. Matsuura, T. Ishikawa, N. Yabuuchi, W. Murata, S. Kuze, *Electrochem. Commun.* **2012**, *21*, 65.
[6] Y. H. Xu, Y. J. Zhu, Y. H. Liu, C. S. Wang, *Adv. Energy Mater.* **2013**, *3*, 128.
[7] M. K. Datta, R. Epur, P. Saha, K. Kadakia, S. K. Park, P. N. Kumt, *J. Power Sources* **2013**, *225*, 316.
[8] Y. Wang, D. W. Su, C. Y. Wang, G. X. Wang, *Electrochem. Commun.* **2013**, *29*, 8.
[9] Y. H. Liu, Y. H. Xu, Y. J. Zhu, J. N. Culver, C. A. Lundgren, K. Xu, C. S. Wang, *ACS Nano* **2013**, *7*, 3627.
[10] D. W. Su, C. Y. Wang, H. J. Ahn, G. X. Wang, *Phys. Chem. Chem. Phys.* **2013**, *15*, 12543.
[11] D. W. Su, H. J. Ahn, G. X. Wang, *Chem. Commun.* **2013**, *49*, 3131.
[12] L. Wu, X. H. Hu, J. F. Qian, F. Pei, F. Y. Wu, R. J. Mao, X. P. Ai, H. X. Yang, Y. L. Cao, *J. Mater. Chem. A.* **2013**, *1*, 7181.
[13] H. L. Zhu, Z. Jia, Y. C. Chen, N. Weadock, J. Y. Wan, O. Vaaland, X. G. Han, T. Li, L. B. Hu, *Nano Lett.* **2013**, *13*, 3093.

[14] Y. M. Lin, P. R. Abel, A. Gupta, J. B. Goodenough, A. Heller, C. B. Mullins, *ACS Appl. Mater. Inter.* **2013**, *5*, 8273.
[15] Y. X. Wang, Y. G. Lim, M. S. Park, S. L. Chou, J. H. Kim, H. K. Liu, S. X. Dou, Y. J. Kim, *J. Mater. Chem. A.* **2014**, *2*, 529.
[16] J. W. Wang, X. H. Liu, S. X. Mao, J. Y. Huang, *Nano Lett.* **2012**, *12*, 5897.
[17] a) J. W. Seo, J. T. Jang, S. W. Park, C. J. Kim, B. W. Park, J. Cheon, *Adv. Mater.* **2008**, *20*, 4269; b) C. X. Zhai, N. Du, H. Zhang, D. R. Yang, *Chem. Commun.* **2011**, *47*, 1270; c) Y. P. Du, Z. Y. Yin, X. H. Rui, Z. Y. Zeng, X. J. Wu, J. Q. Liu, Y. Y. Zhu, J. X. Zhu, X. Huang, Q. Y. Yan, H. Zhang, *Nanoscale* **2013**, *5*, 1456; d) Q. Wu, L. F. Jiao, J. Du, J. Q. Yang, L. J. Guo, Y. C. Liu, Y. J. Wang, H. T. Yuan, *J. Power Sources* **2013**, *239*, 89.
[18] a) B. Luo, Y. Fang, B. Wang, J. S. Zhou, H. H. Song, L. J. Zhi, *Energy Environ. Sci.* **2012**, *5*, 5226; b) Z. F. Jiang, C. Wang, G. H. Du, Y. J. Zhong, J. Z. Jiang, *J. Mater. Chem.* **2012**, *22*, 9494; c) K. Chang, Z. Wang, G. C. Huang, H. Li, W. X. Chen, J. Y. Lee, *J. Power Sources* **2012**, *201*, 259; d) L. Mei, C. Xu, T. Yang, J. M. Ma, L. B. Chen, Q. H. Li, T. H. Wang, *J. Mater. Chem. A.* **2013**, *1*, 8658; e) G. C. Huang, T. Chen, W. X. Chen, Z. Wang, K. Chang, L. Ma, F. H. Huang, D. Y. Chen, J. Y. Lee, *Small* **2013**, *9*, 3693; f) D. Y. Chen, G. Ji, B. Ding, Y. Ma, B. H. Qu, W. X. Chen, J. Y. Lee, *Nanoscale* **2013**, *5*, 7890.
[19] H. K. Jeong, Y. P. Lee, R. J. W. E. Lahaye, M. H. Park, K. H. An, I. J. Kim, C. W. Yang, C. Y. Park, R. S. Ruoff, Y. H. Lee, *J. Am. Chem. Soc.* **2008**, *130*, 1362.
[20] a) C. R. Wang, K. B. Tang, Q. Yang, Y. T. Qian, *Chem. Phy. Lett.* **2002**, *357*, 371; b) H. S. Kim, Y. H. Chung, S. H. Kang, Y. E. Sung, *Electrochim. Acta* **2009**, *54*, 3606.
[21] S. Stankovich, D. A. Dikin, R. D. Piner, K. A. Kohlhaas, A. Kleinhammes, Y. Y. Jia, Y. Wu, S. T. Nguyen, R. S. Ruoff, *Carbon* **2007**, *45*, 1558.
[22] J. Xu, D. H. Lee, R. J. Clément, X. Yu, M. Leskes, A. J. Pell, G. Pintacuda, X. Q. Yang, C. P. Grey, Y. S. Meng, *Chem. Mater.* **2014**, *26*, 1260.
[23] a) S. Komaba, W. Murata, T. Ishikawa, N. Yabuuchi, T. Ozeki, T. Nakayama, A. Ogata, K. Gotoh, K. Fujiwara, *Adv. Funct. Mater.* **2011**, *21*, 3859; b) A. Abouimrane, W. Weng, H. Eltayeb, Y. Cui, J. Niklas, O. Poluektov, K. Amine, *Energy Environ. Sci.* **2012**, *5*, 9632; c) S. M. Oh, S. T. Myung, M. W. Jang, B. Scrosati, J. Hassoun, Y. K. Sun; d) S. Hariharan, K. Saravanan, P. Balaya, *Electrochem. Commun.* **2013**, *31*, 5; e) D. Y. W. Yu, P. V. Prikhodchenko, C. W. Mason, S. K. Batabyal, J. Gun, S. Sladkevich, A. G. Medvedev, O. Lev, *Nat . Comm.* **2013**, *4*, 2922.
[24] W. S. Hummers, R. E. Offeman, *J. Am. Chem. Soc.* **1958**, *80*, 1339.
[25] C. H. Xu, J. Sun, L. Gao, *J. Mater. Chem.* **2012**, *22*, 975.